Giant atom induced zero modes and localization in the nonreciprocal Su-Schrieffer-Heeger chain

Junjie Wang,¹ Fude Li,¹ and X. X. Yi^{1,2,*}

¹Center for Quantum Sciences and School of Physics, Northeast Normal University, Changchun 130024, China

²Center for Advanced Optoelectronic Functional Materials Research,
and Key Laboratory for UV-Emitting Materials and Technology of Ministry of Education,
Northeast Normal University, Changchun 130024, China
(Dated: November 4, 2022)

A notable feature of non-Hermitian systems with skin effects is the sensitivity of their spectra and eigenstates to the boundary conditions. In the literature, three types of boundary conditions—periodic boundary condition, open boundary condition and a defect in the system as a boundary, are explored. In this work we introduce the other type of boundary condition provided by a giant atom. The giant atom couples to a nonreciprocal Su-Schrieffer-Heeger chain at two points and plays the role of defects. We study the spectrum and localization of eigenstates of the system and find that the giant atom can induce asymmetric zero modes. A remarkable feature is that bulk states might localize at the left or the right chain-atom coupling sites in weak localization regimes. This bipolar localization leads to Bloch-like states, even though translational invariance is broken. Moreover, we find that the localization is obviously weaker than the case with two small atoms or open boundary conditions even in strong coupling regimes. These intriguing results indicate that nonlocal coupling of giant atom to a nonreciprocal SSH chain weakens localization of the eigenstates. We also show that the Lyapunov exponent in the long-time dynamics in real space can act as a witness of the localized bulk states.

I. INTRODUCTION

In closed quantum systems, observables like Hamiltonians are represented by Hermitian operators. This is not the case for real systems that are inevitably coupled to environments. It is widely accepted that open quantum systems can be described effectively by non-Hermitian operators on the basis of the quantum trajectory approach. Recently non-Hermitian systems have attracted a plethora of attention [1–7] especially in the field of topological physics. Interesting features are predicted and observed such as the topological insulator laser [8–10], new topological invariants in non-Hermitian systems [11–18], and the breakdown of the conventional bulk-boundary correspondence [19–37].

The systems with non-Hermitian skin effect (NHSE) are very sensitive with respect to boundary conditions. For example, the properties of both spectrum and eigenstates of non-Hermitian systems may change dramatically by changing the boundary conditions from periodic to open ones [21]. In between, a defect introduced into the system could also play the role of boundary [38–42]. Non-Hermitian impurity physics [38] was developed theoretically in a non-reciprocal lattice, where the authors found a new type of steady-state localization characterized by scale-free accumulation of eigenstates with localization lengths proportional to the system size. The scale-free localization can be interpreted by the generalized non-Bloch band theory [39, 40], and strong defectsystem couplings might induce an effective boundary in a periodic system with properties very similar to systems with open boundary condition (OBC) [41–44].

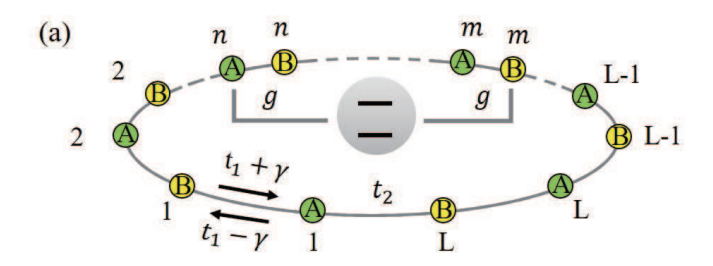
Giant atom such as superconducting qubit has played an important role in superconducting quantum circuits. It can be nonlocally coupled to a waveguide at multiple points [45–

50] and act as an effective boundary for the waveguide. The giant atom might induce chiral bound states for the Hermitian systems of waveguide [48, 49]. These give rise to questions that what properties of the system will change if a giant atom couples to a non-Hermitian topological chain, and what is the difference between giant atom induced localization and that induced by other impurities or defects, and what new physical phenomena would emerge.

In this work, we will answer these questions and focus on spectrum structures and the localization of eigenstates in a system composed of a giant atom and a nonreciprocal Su-Schrieffer-Heeger(SSH) chain. We find that the giant atom can induce asymmetric zero modes. Bulk states may localize at the left or the right chain-atom coupling sites, so we call this "a bipolar localization". Further examination shows that strong atom-chain coupling can not induce transitions from skin-free to skin states in the bulk states. This suggests that the localization is weaker than that with OBC even in strong coupling regimes, and nonlocal couplings weaken localization of the eigenstates. We also show that the feature of localization of the bulk states can be captured by the dynamics in real space.

The paper is organized as follows. In Sec. II, we introduce a model to describe the system composed of a giant atom and a nonreciprocal SSH chain and calculate the spectrum of the system. In Sec. III, we derive an analytical expression for the zero modes induced by giant atom. Two cases, one with two small atoms and the other with a giant atom, are compared and discussed in details. In Sec. IV, we mainly focus on the localization feature of the bulk eigenstates. In Sec. V, we explore the relation between the Lyapunov exponent and the localization of the bulk states. Finally, we summarize our results in Sec. VI.

^{*}Electronic address: yixx@nenu.edu.cn



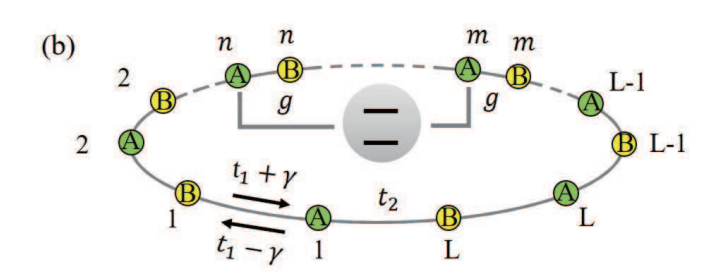


FIG. 1: Sketch of the system. (a) A giant atom coupled to a nonreciprocal SSH chain via A-B coupling. (b) A giant atom coupled to a nonreciprocal SSH chain via A-A coupling.

II. MODEL AND SPECTRUM

As depicted in Figs. 1 (a) and (b), we consider a nonreciprocal SSH chain with periodic boundary conditions (PBC) in real space described by

$$H_{\text{SSH}} = \sum_{l=1}^{L} [(t_1 + \gamma)\hat{C}_{A,l}^{\dagger}\hat{C}_{B,l} + (t_1 - \gamma)\hat{C}_{B,l}^{\dagger}\hat{C}_{A,l} + t_2\hat{C}_{A,l+1}^{\dagger}\hat{C}_{B,l} + t_2\hat{C}_{B,l}^{\dagger}\hat{C}_{A,l+1}],$$
(1)

where the chain consists of L unit cells, and the staggered nearest-neighbor hopping amplitudes are $t_1\pm\gamma$ and t_2 , respectively. The asymmetry of hopping amplitudes $(\gamma\neq 0)$ leads to the non-Hermiticity of the system. $\hat{C}_{A(B),l}^{\dagger}$ and $\hat{C}_{A(B),l}$ are the creation and annihilation operators for the sublattice site A(B) at site l. To have an effective boundary, we introduce a two level giant atom coupling at two points to a nonreciprocal SSH chain via A-B (or A-A) couplings. The interaction Hamiltonian for such a system can be written as

$$H_{I,AB} = g|e\rangle\langle g|(\hat{C}_{A,n} + \hat{C}_{B,m}) + \text{H.c.},$$

 $H_{I,AA} = g|e\rangle\langle g|(\hat{C}_{A,n} + \hat{C}_{A,m}) + \text{H.c.},$ (2)

where g denotes the atom-chain coupling strength. $|g\rangle$ and $|e\rangle$ are the ground state and the excited state of the giant atom, respectively. The Hamiltonians of atom-chain coupling read

$$H_{AB} = H_{SSH} + H_{I,AB}, \tag{3a}$$

$$H_{AA} = H_{\text{SSH}} + H_{LAA}. \tag{3b}$$

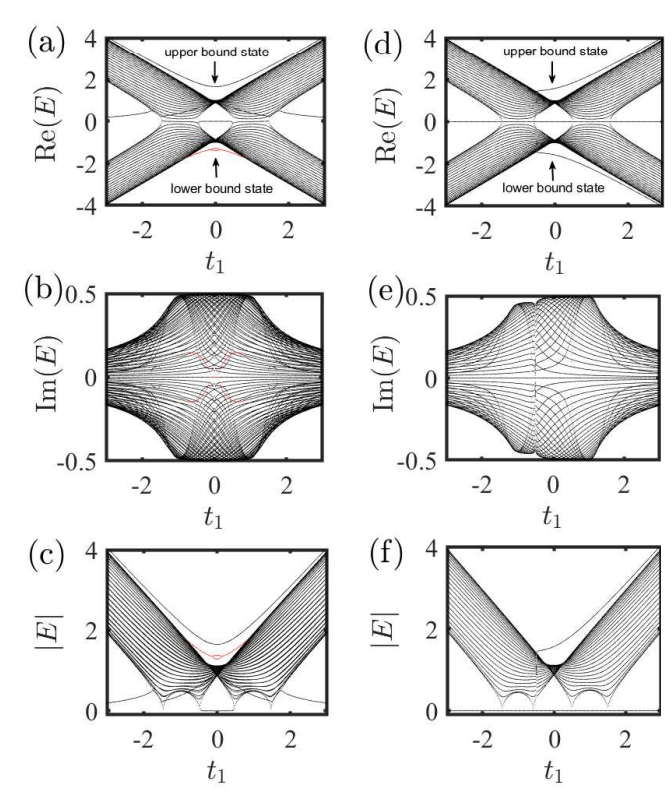


FIG. 2: Spectrum as a function of t_1 in (a,b,c) with A-B and (d,e,f) with A-A coupling, respectively. First (second) row show real (imaginary) part of the spectrum, while last row shows absolute value of the spectrum. The results are obtained by numerically solve the Schödinger equation. The chosen parameters are $L=50, m=26, n=25, g=1, t_1=0.2, t_2=1$, and $\gamma=0.5$.

In the single-excitation subspace, the eigenstate of the Bloch Hamiltonian can be expressed as

$$|\psi\rangle = U_e|e,G\rangle + \sum_k A_k \hat{C}_{A,k}^{\dagger}|g,G\rangle + \sum_k B_k \hat{C}_{B,k}^{\dagger}|g,G\rangle$$
(4)

where $|G\rangle$ denotes the ground state of the SSH chain. Making use of the time-independent Schrödinger equation $H(k)|\psi\rangle=E|\psi\rangle$, we obtain the eigenvalues of the system with A-B couplings

$$E = \frac{g^2}{\pi} \int_{-\pi}^{\pi} dk (E + t_1 \cos[k(m-n)] - \gamma \sin[k(m-n)] + t_2 \cos[k(m-n+1)]) / (E^2 - \omega_k^2),$$
(5)

with

$$\omega_k = \sqrt{(t_1 + \gamma + t_2 e^{-ik})(t_1 - \gamma + t_2 e^{ik})}.$$
 (6)

Setting E=0, we can derive a condition for the emergence of the zero mode, i.e., $t_1\in[-t_2+\gamma,t_2-\gamma]$. In the absence of giant atoms, the different topological phases for nonreciprocal SSH model can be distinguished by the winding number [16] $v=\frac{1}{\pi}\int_{-\pi}^{\pi}dk\left\langle \phi^L\left|i\partial_k\right|\phi^R\right\rangle$. It satisfies v=1 for $t_1\in[-t_2+\gamma,t_2-\gamma]$. Note that the condition

for the emergence of the zero mode is identical to the nontrivial phase boundary of systems without giant atoms. (See Appendix A for analytical results and Fig. 2 (a-c) for numerical simulations). Except for the modes in the energy gap, there are other eigenvalues outside (lying above and below) the continuous bands as shown in Fig. 2 (a). We call the corresponding eigenstates upper and lower bound states, respectively. Interestingly, eigenvalues form a close circle (red loop) in Fig. 2 (c), because the system crosses two exception points as the increase of parameter t_1 . Combined with Fig. 2 (a,b), it is clearly shown that complex conjugate pair of eigenvalues become purely real when crossing the left exception point, and adjacent real eigenvalues merge into complex conjugate pairs when crossing the right exception point.

For A-A coupling, the eigenvalue satisfies

$$E = \frac{2g^2}{L} \sum_{k} \left(\frac{E(1 + \cos[k(m-n)])}{E^2 - \omega_k^2} \right).$$
 (7)

Obviously, E=0 is always the solution of Eq. (7), which can be seen in the numerical spectra of Hamiltonian H_{AA} (Fig. 2 (d-f)). In Fig. 2 (d), we find that the upper and lower eigenvalues merge into the continual band as t_1 decreases, which indicates that the corresponding bound states vanished.

III. ZERO MODE AND BOUND STATES

The probability distributions of the system at zero modes and upper bound states as a function of lattice site N with different parameters are shown in Fig. 3 for A-B coupling and in Fig. 4 for A-A coupling. The probability distribution on giant atom is set at N=2L+1=101. The bars represent the numerical results and the empty circles represent the analytical results. Simple algebra shows that the analytical results of the probability distributions of bound states with energy E take (see Appendix B for details)

$$\frac{A_l}{U_e} = \frac{(-1)^{y+1} \left(T \tau_1^{|l-n|} + g \tau_2^{|l-m-1|} + Y_2 \tau_2^{|l-m|} \right)}{\sqrt{x^2 - 4(t_1 + \gamma)(t_2 - \gamma)}}, \quad (8a)$$

$$\frac{B_l}{U_e} = \frac{(-1)^{y+1} \left(T \tau_2^{|l-m|} + g \tau_1^{|l-n+1|} + Y_1 \tau_1^{|l-n|} \right)}{\sqrt{x^2 - 4(t_1 + \gamma)(t_1 - \gamma)}}$$
 (8b)

for the A - B coupling, and

$$\frac{A_l}{U_e} = \frac{(-1)^{y+1}T}{\sqrt{x^2 - 4(t_1 + \gamma)(t_1 - \gamma)}} \left(\tau_1^{|l-n|} + \tau_3^{|l-m|}\right), \quad (9a)$$

$$\frac{B_l}{U_e} = \frac{(-1)^{y+1}}{\sqrt{x^2 - 4(t_1 + \gamma)(t_1 - \gamma)}} \left\{ Y_1 \left(\tau_1^{|l-n|} + \tau_3^{|l-m|} \right) + g \left(\tau_1^{|l-n+1|} + \tau_3^{|l-m+1|} \right) \right\}$$
(9b)

for the A-A coupling. Here, $y=\theta(x)$ is the step function,

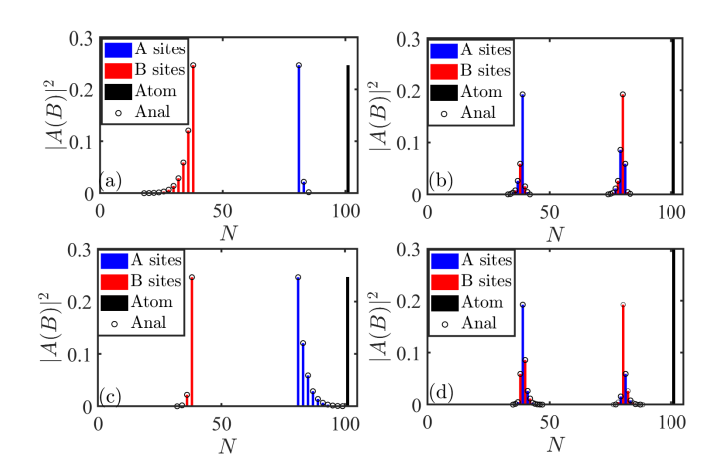


FIG. 3: The probability distributions of bound states for the system (3a) with A-B coupling as a function of lattice site N. (a) and (c) are plotted for the probability distribution of zero mode. (b) and (d) are plotted for the probability distribution of the upper bound state. Here, $t_1=0.2$ in (a-b), and $t_1=-0.2$ in (c-d). The other parameters are chosen as $L=50, m=40, n=20, g=1, t_2=1,$ and $\gamma=0.5$.

and $x=(E^2-(t_1+\gamma)(t_1-\gamma)-t_2^2)/t_2$. We define $T=gE/t_2,\,Y_{1(2)}=g(t_1\mp\gamma)/t_2,\,\tau_1=a\,(b)$ for $l\geq n\,(l< n),\,\tau_2=a\,(b)$ for $l>m\,(l\leq m),\,\tau_3=a\,(b)$ for $l\geq m\,(l< m),\,$ and $a=(x\pm\sqrt{x^2-4(t_1+\gamma)(t_1-\gamma)})/2(t_1+\gamma),b=(x\pm\sqrt{x^2-4(t_1+\gamma)(t_1-\gamma)})/2(t_1-\gamma)$ with +(-) corresponding to $x<-2|t_1|\,(x>2|t_1|)$.

For the system with A-B coupling, the zero mode present in the bulk topological non-trivial phase of nonreciprocal SSH model with $-t_2 + \gamma < t_1 < t_2 - \gamma$. Setting E=0, the probability distribution of the zero mode can be obtain from Eqs. (8a) and (8b),

$$A_{l}/U_{e} = Y_{3} \times \begin{cases} \left(-\frac{t_{1}-\gamma}{t_{2}}\right)^{(l-m)}, & (l>m), \\ 0, & (l\leq m), \end{cases}$$

$$B_{l}/U_{e} = Y_{4} \times \begin{cases} \left(-\frac{t_{1}+\gamma}{t_{2}}\right)^{(n-l)}, & (l< n), \\ 0, & (l\geq n), \end{cases}$$
(10)

where $Y_3=g/(t_1-\gamma)$, and $Y_4=g/(t_1+\gamma)$. We find that the probability amplitudes in the wave function satisfy the asymmetrical distribution $|A_l|\neq |B_{m+n-l}|$. Assuming $\gamma>0$, we have $|(t_1-\gamma)/t_2|<|(t_1+\gamma)/t_2|$ for $t_1>0$, and $|(t_1+\gamma)/t_2|<|(t_1-\gamma)/t_2|$ for $t_1<0$, which suggests that the system mainly occupies B sites on the left side of the giant atom when $t_1>0$, and occupies the A sites on the right side of the giant atom when $t_1<0$. Obviously, the spatial distributions of wave functions on the left and right sides of the giant atom are the same for the critical point with $t_1=0$. Besides, as the increase of g, the probability of the system occupying the giant atom are gradually suppressed, but the spatial symmetry of zero modes on the SSH chain can not be changed.

In Figs. 3(a) and 3(c), we show the probability distributions of zero modes for A-B coupling as a function of lattice site

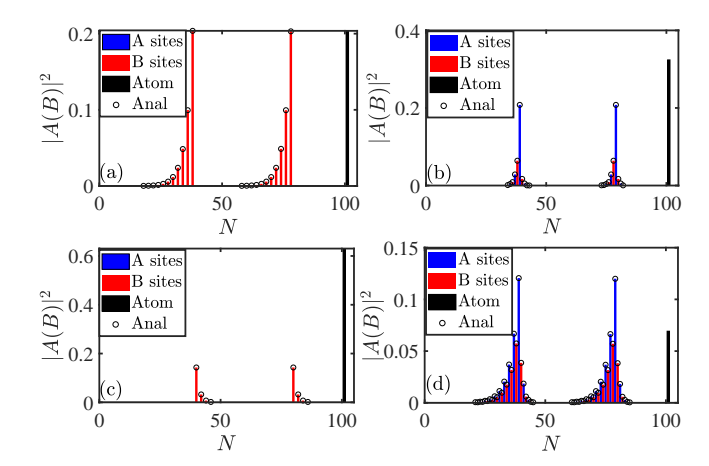


FIG. 4: The probability distributions of the system (3b) in bound states with A-A coupling as a function of lattice site N. (a) and (c) are plotted for the probability distribution of zero mode, and corresponding wave functions do not distribute on A sites. (b) and (d) are plotted for the probability distribution of the upper bound state. The system in the bulk topological non-trivial phase with $t_1=0.2$ in (a-b) and the bulk topological trivial phase with $t_1=1.6$ in (c-d). The other parameters are set as $L=50, m=40, n=20, g=1, t_2=1,$ and $\gamma=0.5$.

N with $t_1=0.2$ and $t_1=-0.2$, respectively. In this case, the zero modes mainly locate on the left (right) sides of the giant atom with $t_1=0.2$ ($t_1=-0.2$), and satisfy the chiral symmetry [48]. It is clear that the analytical results given by Eq. (10) are in good agreement with the numerical results. In Figs. 3(b) and 3(d), we show the corresponding distributions of the upper bound state with $t_1=0.2$ and $t_1=-0.2$, respectively. Although the amplitude distributions of wave function on sites are lack of spatial symmetry, the non-reciprocity can induce a supremacy that makes the upper bound states to distribute on the left (right) of coupling point more than the right (left) of coupling point for $t_1=0.2$ ($t_1=-0.2$). Similarly, the analytical results given by Eq. (8a) and Eq. (8b) are in good agreement with the numerical results.

For the system with A-A coupling, zero modes are always there regardless of the value of t_1 . According to Eq. (9a) and Eq. (9b), we can get the probability distribution of the zero mode, which gives rise to $A_l=0$, and

$$B_{l}/U_{e} = Y_{4} \times \begin{cases} \left(\frac{-t_{1}-\gamma}{t_{2}}\right)^{(n-l)} + \left(\frac{-t_{1}-\gamma}{t_{2}}\right)^{(m-l)}, & (l < n), \\ \left(\frac{-t_{1}-\gamma}{t_{2}}\right)^{(m-l)}, & (n \leq l < m), \\ 0, & (m \leq l), \end{cases}$$

in the bulk topological non-trivial phase of the SSH model with $-t_2+\gamma < t_1 < t_2-\gamma$ and

$$B_{l}/U_{e} = -Y_{4} \times \begin{cases} 0, & (l < n), \\ \left(\frac{-t_{2}}{t_{1} + \gamma}\right)^{l - n}, & (n \le l < m), \\ \left(\frac{-t_{2}}{t_{1} + \gamma}\right)^{l - n} + \left(\frac{-t_{2}}{t_{1} + \gamma}\right)^{l - m}, & (m \le l), \end{cases}$$
(12)

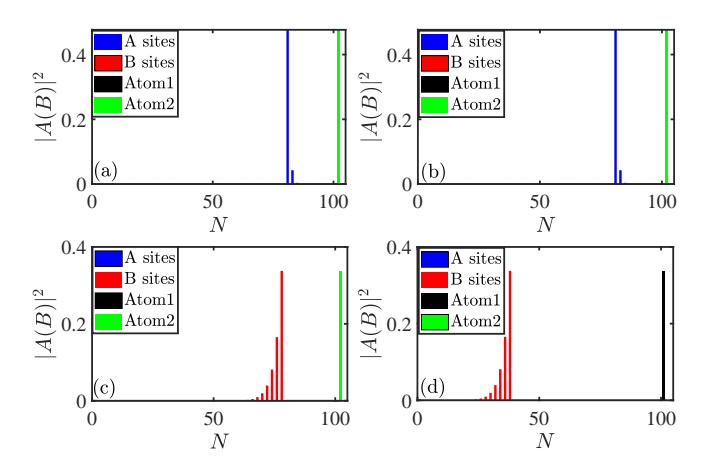


FIG. 5: The probability distributions of zero modes for the system that two small atoms couple to a nonreciprocal SSH chain as a function of lattice site N. (a) and (b) are plotted for the A-B coupling. (c) and (d) are plotted for the A-A coupling. Here, $L=50, m=40, n=20, g=1, t_1=0.2, t_2=1,$ and $\gamma=0.5$.

in the bulk topological trivial phase of the SSH model with $t_1 > t_2 + \gamma$ or $t_1 < -t_2 - \gamma$. As for $-t_2 - \gamma < t_1 < \tau$ $-t_2 + \gamma$ and $-t_2 - \gamma < t_1 < -t_2 + \gamma$, the analytical results of zero model are not given. Note that the amplitudes of the wave functions only distribute on B sites on the left sides of the giant atom or between two coupling points with $-t_2$ + $\gamma < t_1 < t_2 - \gamma$, and distribute on B sites on the right sides of the giant atom or between two coupling points with $t_1 >$ $t_2 + \gamma$ or $t_1 < -t_2 - \gamma$. Similarly, distributions of wave function can also be changed by tuning the parameters of the system. Taking t_1 t_2 and γ to be positive leads to γ/t_2 < $|(t_1 + \gamma)/t_2| < 1$ in the bulk topological non-trivial phase, and $0 < |t_2/(t_1 + \gamma)| < t_2/(t_2 + 2\gamma)$ in the bulk topological trivial phase. Taking $t_2 \leq 2\gamma$ yields $\gamma/t_2 \geq t_2/(t_2+2\gamma)$. This indicates that the decay of distributions in the bulk topological non-trivial phase are always slower than the bulk topological trivial phase.

In order to verify the above analysis, in Figs. 4(a) and 4(c), we show the probability distributions of zero modes for A-A coupling as a function of lattice site N with $t_1=0.2$ and $t_1=1.6$, respectively. The results in Figs. 4(a) and 4 (c) are obtained by numerical simulations and they show that $|B_l|\approx |B_{l+m-n}|$ are satisfied. The decay of distributions with $t_1=0.2$ are slower than the distributions with $t_1=1.6$. In Figs. 3(b) and 3(d), we show the corresponding distributions of the upper bound state with $t_1=0.2$ and $t_1=1.6$, respectively. It is easy to find that they satisfy $|A(B)_l|\approx |A(B)_{l+m-n}|$, and the non-reciprocity makes upper bound states to distribute on the left of coupling point more than the right of coupling point.

In Fig. 3 and Fig. 4, we present rich and intriguing zero modes for the system composed of a giant atom and a non-reciprocal SSH chain. Note that zero modes localize at two effective boundaries. While for a nonreciprocal SSH chain with OBC, zero modes only localize at one of the two boundaries [21]. These two cases are different, because giant atom not only induces two effective boundaries, but also couples

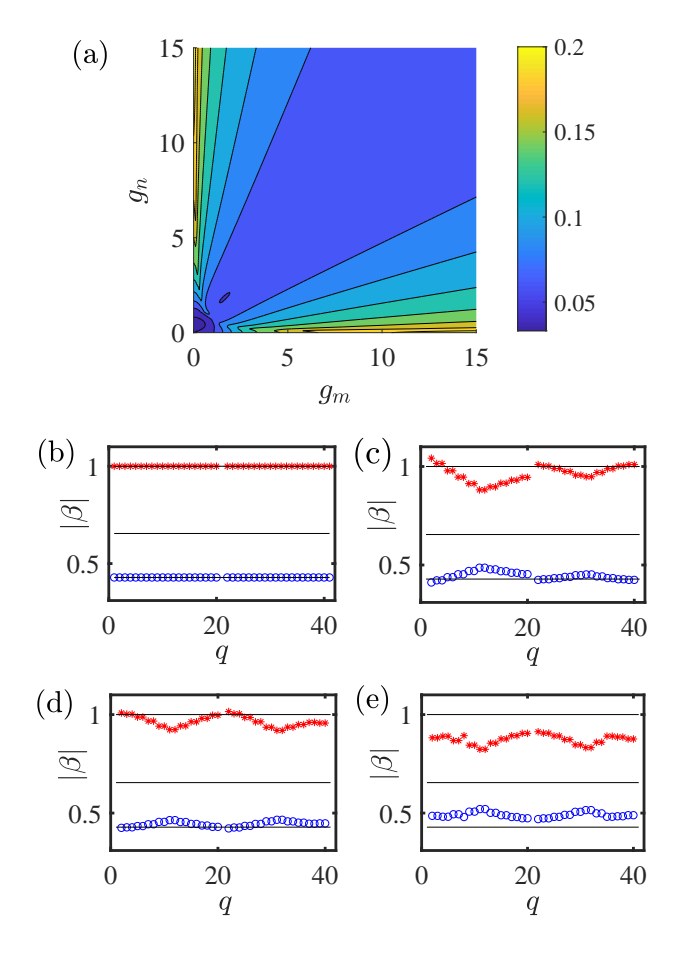


FIG. 6: (a) $\overline{\text{IPR}}$ on the parameter space of g_m and g_n for the system (3a) with A-B coupling given by Eq. (13). (b-e) $|\beta_1|$ (red star) and $|\beta_2|$ (blue circle) as a function of q given by Eq. (15) with $(g_m,g_n)=(0,0),(1,1),(13,13),$ and (13,1), respectively. The three reference lines from top to bottom correspond to $|\beta|=1,\sqrt{|(t_1-\gamma)/(t_1+\gamma)|},$ and $|(t_1-\gamma)/(t_1+\gamma)|$. The parameters shared by all of the figures are $L=20, m=n=10, t_1=0.2, t_2=1,$ and $\gamma=0.5.$

them. In order to show the validity of the above conclusions, we plot the probability distributions of zero modes for the system that two small atoms couple to a nonreciprocal SSH chain. The coupling points locate at sites m and n, respectively. As shown in Fig. 5, there are two zero modes for small-atom case. Both modes localize at the right coupling point for A-A coupling, and one for each coupling point for A-B coupling with $m=40, n=20, g=1, t_1=0.2, t_2=1$, and $\gamma=0.5$. It is clearly shown that although two small atoms as defects induce two effective boundaries, zero modes localize at only one of the two boundaries. Note that this case is similarly to the zero mode with OBC. Hence, it can be seen that the zero modes for systems with giant atom are very unique, because nonlocal couplings weaken the localization.

IV. LOCALIZATION OF EIGENSTATES

Our aim is to study the localization of eigenstates, and we only interest in the wave functions living at the SSH chain, so distributions on the giant atom are not considered. To this aim, we calculate the modified averaged inverse participation ratio $\overline{\rm IPR}$,

$$\overline{IPR} = \frac{1}{N} \sum_{q=1}^{N} IPR_q$$
 (13)

with ${\rm IPR}_q = \sum_{N=1}^{2L} |\psi_N^q|^4/(\sum_{N=1}^{2L} |\psi_N^q|^2)^2$ and ψ_N^q is the probability amplitude at site N of the qth right eigenstate of Hamiltonian in real space. $\overline{\rm IPR}$ will enhance as the increase of the localization. In Fig. 6 (a), we show $\overline{\rm IPR}$ on the parameter space of g_m and g_n for the giant-atom case with A-B coupling (A-A coupling is similar). g_m and g_n are the atomchain coupling strength, where m and n denote the coupling sites. Note that $\overline{\rm IPR}$ is suppressed when $g_m=g_n$, and can be lifted as the increase of $\delta g=|g_n-g_m|$, which indicates that the localization will be suppressed for the same coupling strength setting. Particularly, for the case of $g_n \neq 0$ ($g_m=0$) or $g_m \neq 0$ ($g_n=0$), i.e., like a small-atom case, $\overline{\rm IPR}$ will significant enhance as the increase of g_n or g_m , which suggests that nonlocal couplings weaken localization of eigenstates for giant-atom case.

In the last section, we have shown the behavior of the bound states. Next, to analyze the localization of bulk states in detail, let us consider the real-space eigen-equation of the system. In the bulk of chain, it satisfies

$$t_2 \psi_{B,l-1} + [t_1 + \gamma] \psi_{B,l} = E \psi_{A,l}, [t_1 - \gamma] \psi_{A,l} + t_2 \psi_{A,l+1} = E \psi_{B,l}.$$
 (14)

With $(\psi_{A,l},\psi_{B,l})=\beta^l(\psi_A,\psi_B)$, it yields

$$\beta_{1,2}(E) = \frac{\left[\Delta \pm \sqrt{\Delta^2 - 4t_2^2(t_1^2 - \gamma^2)}\right]}{2t_2(t_1 + \gamma)},\tag{15}$$

where $\Delta=E^2+\gamma^2-t_1^2-t_2^2$, and +(-) corresponds to β_1 (β_2). In Fig. 6(b-e), we show $|\beta_1|$ (red star) and $|\beta_2|$ (blue circle) as a function of q with different coupling strengths $(g_m, g_n) = (0, 0), (1, 1), (13, 13), \text{ and } (13, 1).$ For the system under OBC without giant atom, $|\beta_{1,2}| =$ $\sqrt{|(t_1-\gamma)/(t_1+\gamma)|}$ [21] corresponds to the line in the middle, and the wave functions take the form of skin states. While for the system under PBC without giant atom, $|\beta_1| = 1$, $|\beta_2| = |(t_1 - \gamma)/(t_1 + \gamma)|$ corresponds to the line in the above and below, respectively, and the wave functions take the form of skin-free states. When coupling strengths $g_m = g_n = 0$, the bulk states obviously take the form of skin-free states (Fig. 6 (b)). Counter-intuitively, $|\beta_{1,2}|$ cross the line in the above and below, respectively as $g_m = g_n = 1 (or \ 13)$ (Fig. 6 (c-d)), which suggests that bulk states might localize at the left $(|\beta_1| > 1)$ or the right $(|\beta_1| < 1)$ chain-atom coupling sites as long as coupling strengths are the same. Note that eigenstates are in a relatively weak localization regime in this case (Fig. 6 (a)). This bipolar localization inevitably leads to Bloch-like

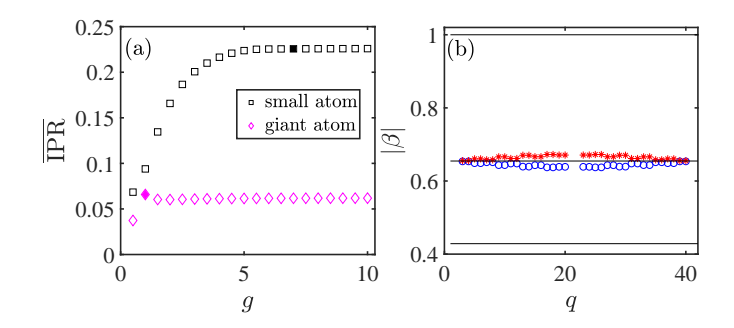


FIG. 7: (a) $\overline{\text{IPR}}$ as a function of g given by Eq. (13) for the system that a giant atom (magenta rhombus) or two small atoms (black square) coupls to a nonreciprocal SSH chain. (b) $|\beta_1|$ (red star) and $|\beta_2|$ (blue circle) as a function of q given by Eq. (15) with g=7 corresponds to black filled square in (a). The parameters are chosen as $L=20, m=n=10, t_1=0.2, t_2=1$, and $\gamma=0.5$.

states albeit broken translational invariance, but the bipolar localization will disappear in a relatively strong localization regime $(g_m, g_n) = (13, 1)$ as shown in Fig. 6 (e).

In order to further illustrate that nonlocal couplings have significant effect on the localization of eigenstates, we show $\overline{\text{IPR}}$ as a function of the coupling strengths $g_m = g_n = g$ for the system that a giant atom or two small atoms couples to a nonreciprocal SSH chain in Fig. 7(a). Note that $\overline{\text{IPR}}$ for giant-atom case reaches peak at g=1 corresponding to magenta filled rhombus in Fig. 7(a), and even higher than the case with a bigger g. Comparing to small-atom case, it clear that nonlocal coupling weakens localization of eigenstates.

In Fig. 7 (b), we show $|\beta_1|$ (red star) and $|\beta_2|$ (blue circle) as a function of q with g=7 for small-atom case, and corresponding to black filled square in Fig. 7 (a). It can be seen that $|\beta_{1,2}| \approx \sqrt{|(t_1-\gamma)/(t_1+\gamma)|}$ are similar to the case with OBC, which implies that bulk states are like the form of skin states. On the contrary, it can not be realized for giant-atom case even for a bigger g=13 as shown in Fig. 6 (d).

V. LYAPUNOV EXPONENT

In order to predict the localization of bulk states, we calculate the Lyapunov exponent $\lambda(v)$ in the long-time dynamics in real space far from edges,

$$\lambda(v) = \lim_{t \to \infty} \frac{\log |\psi(t)|}{t},\tag{16}$$

where the amplitude $|\psi(t)\rangle=A_{(L+1)/2+n}(t)$ [or similarly $|\psi(t)\rangle=B_{(L+1)/2+n}(t)$] varies along the spacetime path n=vt, and v is the drift velocity [51–53]. Recent research shows that if $\lambda(v)$ does not reach its largest value at zero drift velocity, then the non-Hermitian system exhibits the NHSE [53]. Clearly, Lyapunov exponent can act as a witness of defect-induced localized bulk states in the same way. For example, the existence of giant atom induced localized bulk states can be captured by the Lyapunov exponent exhibiting its largest value at a nonvanishing drift velocity.

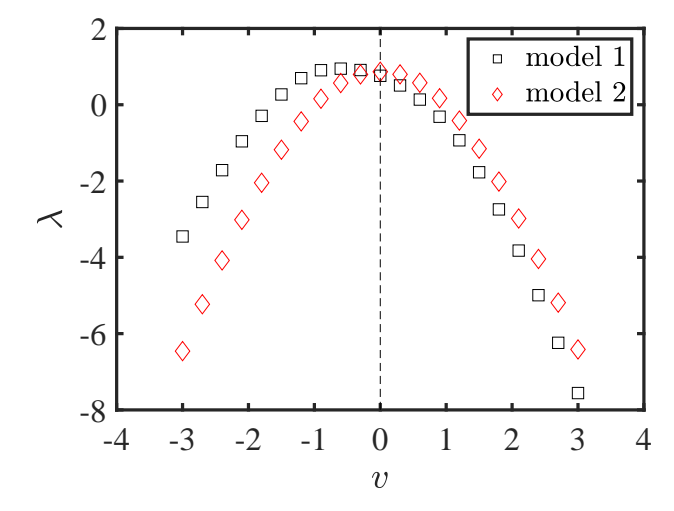


FIG. 8: Lyapunov exponent $\lambda(v)$ as a function of v given by Eq. (16) for the system (3a) (black squares) or the system (17) (red diamonds) with A-B coupling, respectively. The parameters are set as $L=401, m=n=1, t_1=0.6, t_2=1, \gamma=1$, and $\delta=1$.

The Lyapunov exponent in the long-time dynamics is numerically computed by solving the time-dependent Schrödinger equation. In Fig. 8, model 1 with localized bulk states corresponds to the nonreciprocal system (3a) with $A\!-\!B$ coupling ($A\!-\!A$ coupling is similar). As a comparison, model 2 without localized bulk states is described by

$$H'_{AB} = H'_{SSH} + H_{I,AB},$$
 (17)

with

$$H'_{SSH} = \sum_{l=1}^{L} [t_1 \hat{C}_{A,l}^{\dagger} \hat{C}_{B,l} + t_1 \hat{C}_{B,l}^{\dagger} \hat{C}_{A,l} + t_2 \hat{C}_{A,l+1}^{\dagger} \hat{C}_{B,l} + t_2 \hat{C}_{B,l}^{\dagger} \hat{C}_{A,l+1} + i\delta \hat{C}_{A,l}^{\dagger} \hat{C}_{A,l} - i\delta \hat{C}_{B,l}^{\dagger} \hat{C}_{B,l}],$$
(18)

where gain or loss $(\pm i\delta)$ of the sublattice A(B) leads to non-Hermiticity. The initial state is prepared in the bulk of the

lattice, i.e., $A_{(L+1)/2+n}(0)=B_{(L+1)/2+n}(0)=\delta_{n,0}$, and we chose a long lattice (L=401) to avoid the wave packet reach-

ing the effective boundary at the observation time t=50. This time is sufficient to compute $\lambda(v)$ with good accuracy. It is clearly shown that Lyapunov exponent exhibiting its largest value at a nonvanishing drift velocity can act as a witness of the existence of localized bulk states.

VI. SUMMARY

In summary, we have studied a giant atom coupled to two points of a nonreciprocal SSH chain. We show the spectrum structures of the system, and give a condition for the emergence of the zero mode. The interplay of nonreciprocal hopping and the nonlocal couplings can induce asymmetric zero modes. It is clear that the analytical results of zero modes are precise and almost identify with the numerical results. The features of zero modes are unique and obviously different from the case with OBC or two small atoms. Counterintuitively, we uncover that bulk states might localize at the left or the right chain-atom coupling sites in weak localization regimes, and the localization is obviously weaker than the case with small-atom or OBC even in strong coupling regimes. The above results suggest that nonlocal coupling of giant atoms to a nonreciprocal SSH chain weakens localization of both zero modes and bulk states. We also show that Lyapunov exponent exhibiting its largest value at a nonvanishing drift velocity can act as a witness of the localized bulk states.

VII. ACKNOWLEDGMENTS

The authors acknowledge Weijun Cheng for helpful comments. This work was supported by the National Natural Science Foundation of China (NSFC) under Grants No. 12175033, No. 12147206 and National Key R&D Program of China (No. 2021YFE0193500).

Appendix A: energy equation

Consider a system consisting of a giant atom coupled to a nonreciprocal SSH chain via A-B coupling, the Hamiltonian of the system in the momentum space reads,

$$\begin{split} H_{AB}(k) = & H_{\text{SSH}}(k) + H_{I,AB}(k) \\ = & \sum_{k} [[(t_1 + \gamma) + t_2 e^{-ik}] \hat{C}_{A,k}^{\dagger} \hat{C}_{B,k} + [(t_1 - \gamma) \\ & + t_2 e^{ik}] \hat{C}_{B,k}^{\dagger} \hat{C}_{A,k}] + \frac{g}{\sqrt{L}} \sum_{k} [|e\rangle\langle g| (\hat{C}_{A,k} e^{ikn} \\ & + \hat{C}_{B,k} e^{ikm}) + \text{H.c.}]. \end{split}$$
(A1)

The time-independent Schödinger equation $H_{AB}(k)|\psi\rangle=E|\psi\rangle$ together with Eq. (4) leads to,

$$EU_e = \frac{g}{\sqrt{L}} \sum_k \left(A_k e^{ikn} + B_k e^{ikm} \right),$$

$$EA_k = \left(t_1 + \gamma + t_2 e^{-ik} \right) B_k + \frac{g}{\sqrt{L}} e^{-ikn} U_e, \quad (A2)$$

$$EB_k = \left(t_1 - \gamma + t_2 e^{ik} \right) A_k + \frac{g}{\sqrt{L}} e^{-ikm} U_e.$$

Eliminating A_k , B_k and U_e in Eq. (A2), we obtain the equation for E,

$$E = \frac{2g^2}{L} \sum_{k} (E + t_1 \cos[k(m-n)] - \gamma \sin[k(m-n)]$$

$$+ t_2 \cos[k(m-n+1)]) / (E^2 - \omega_k^2)$$

$$= \frac{g^2}{\pi} \int_{-\pi}^{\pi} dk (E + t_1 \cos[k(m-n)] - \gamma \sin[k(m-n)]$$

$$+ t_2 \cos[k(m-n+1)]) / (E^2 - \omega_k^2).$$
(A3)

To obtain the zero-mode, we set E=0 and write $z_1=e^{ik}$ and $z_2=e^{-ik}$, the right-hand side of the last equation can be simplified via Residue theorem (although E=0, we keep it in the equation for clarity of expression)

$$\frac{g^2}{\pi} \int_{-\pi}^{\pi} dk (E + t_1 \cos[k(m-n)] - \gamma \sin[k(m-n)] + t_2 \cos[k(m-n+1)]) / (E^2 - \omega_k^2)$$

$$= \frac{-g^2}{2\pi i} \left[\oint_{|z_1|=1} dz_1 \frac{(t_1 - \gamma)z_1^{m-n} + t_2 z_1^{m-n+1}}{(t_1 + \gamma)t_2(z_1 + \frac{t_2}{t_1 + \gamma})(z_1 + \frac{t_1 - \gamma}{t_2})} + \oint_{|z_2|=1} dz_2 \frac{(t_1 + \gamma)z_2^{m-n} + t_2 z_2^{m-n+1}}{(t_1 - \gamma)t_2(z_2 + \frac{t_2}{t_1 - \gamma})(z_2 + \frac{t_1 + \gamma}{t_2})} \right]$$

$$= \begin{cases}
\frac{-g^2}{t_1 - \gamma} \left(\frac{-t_2}{t_1 - \gamma} \right)^{m-n}, & (-t_2 - \gamma < t_1 < -t_2 + \gamma), \\
0, & (-t_2 + \gamma < t_1 < t_2 - \gamma), \\
\frac{-g^2}{t_1 + \gamma} \left(\frac{-t_2}{t_1 - \gamma} \right)^{m-n}, & (t_1 < -t_2 - \gamma, \\
+ \frac{-g^2}{t_1 + \gamma} \left(\frac{-t_2}{t_1 + \gamma} \right)^{m-n}, & or \ t_1 > t_2 + \gamma).
\end{cases}$$

Clearly, when $-t_2 + \gamma < t_1 < t_2 - \gamma$, we can find the zero mode E=0.

Similarly, for the system with A-A coupling, the interaction Hamiltonian in the momentum space reads

$$H_{I,AA}(k) = \frac{g}{\sqrt{L}} \sum_{k} |e\rangle \langle g| \hat{C}_{A,k} \left(e^{ikn} + e^{ikm} \right) + \text{H.c.},$$
(A5)

and $H_{AA}(k)|\psi\rangle = E|\psi\rangle$ leads to

$$EU_e = \frac{g}{\sqrt{L}} \sum_k A_k \left(e^{ikn} + e^{ikm} \right),$$

$$EA_k = \left(t_1 + \gamma + t_2 e^{-ik} \right) B_k + \frac{g}{\sqrt{L}} \left(e^{-ikn} + e^{-ikm} \right) U_e,$$

$$EB_k = \left(t_1 - \gamma + t_2 e^{ik} \right) A_k.$$
(A6)

Some algebras shows that the energy E satisfies

$$E = \frac{2g^2}{L} \sum_{k} \left(\frac{E(1 + \cos[k(m-n)])}{E^2 - \omega_k^2} \right). \tag{A7}$$

Evidently, E = 0 is always the solution of the Eq. (A7).

Appendix B: states outside the band

For the system with A - B couplings, in accordance to the Eq. (A2), the probability amplitudes A_k and B_k satisfy,

$$A_{k}/U_{e} = \frac{g}{\sqrt{L}t_{2}} \left(Ee^{-ikn} + \left(t_{1} + \gamma + t_{2}e^{-ik} \right) e^{-ikm} \right) f(k),$$

$$B_{k}/U_{e} = \frac{g}{\sqrt{L}t_{2}} \left(Ee^{-ikm} + \left(t_{1} - \delta + t_{2}e^{ik} \right) e^{-ikn} \right) f(k),$$

where $f(k) = 1/(x - (t_1 + \gamma)e^{ik} - (t_1 - \gamma)e^{-ik})$ and $x = (E^2 - (t_1 + \gamma)(t_1 - \gamma) - t_2^2)/t_2$. By Fourier expansion for f(k),

$$f(k) = a_0 + \sum_{p} \left[\left(\frac{a_p - ib_p}{2} \right) e^{ikp} + \left(\frac{a_p + ib_p}{2} \right) e^{-ikp} \right],$$
(B2)

with

$$a_{0} = \frac{1}{2\pi} \int_{-\pi}^{\pi} f(k)dk,$$

$$\frac{a_{p} + ib_{p}}{2} = \frac{1}{2\pi} \int_{-\pi}^{\pi} f(k)e^{ikp}dk,$$

$$\frac{a_{p} - ib_{p}}{2} = \frac{1}{2\pi} \int_{-\pi}^{\pi} f(k)e^{-ikp}dk,$$
(B3)

we derive f(k) as follows

$$f(k) = \frac{(-1)^{y+1}}{\sqrt{x^2 - 4(t_1 + \gamma)(t_1 - \gamma)}} \left[1 + \sum_{p=1}^{L} \left(e^{-ikp}a^p + e^{ikp}b^p\right)\right],$$

where $y=\theta(x)$ is the step function, and $a=(x+\sqrt{x^2-4(t_1+\gamma)(t_1-\gamma)})/2(t_1+\gamma), b=(x+\sqrt{x^2-4(t_1+\gamma)(t_1-\gamma)})/2(t_1-\gamma)$ for $x<-2|t_1|$ or $a=(x-\sqrt{x^2-4(t_1+\gamma)(t_1-\gamma)})/2(t_1+\gamma), b=(x-\sqrt{x^2-4(t_1+\gamma)(t_1-\gamma)})/2(t_1-\gamma)$ for $x>2|t_1|$. Substituting the above results into Eq. (B1), we will get the probability amplitude in real space by inverse Fourier transformation. The result is,

$$A_{l}/U_{e} = \frac{1}{\sqrt{L}} \sum_{k} e^{ikl} A_{k}/U_{e}$$

$$= \frac{(-1)^{y+1} \left(T\tau_{1}^{|l-n|} + g\tau_{2}^{|l-m-1|} + Y_{2}\tau_{2}^{|l-m|} \right)}{\sqrt{x^{2} - 4(t_{1} + \gamma)(t_{2} - \gamma)}}, \quad (B5)$$

$$B_{l}/U_{e} = \frac{1}{\sqrt{L}} \sum_{k} e^{ikl} B_{k}/U_{e}$$

$$= \frac{(-1)^{y+1} \left(T\tau_{2}^{|l-m|} + g\tau_{1}^{|l-n+1|} + Y_{1}\tau_{1}^{|l-n|} \right)}{\sqrt{x^{2} - 4(t_{1} + \gamma)(t_{1} - \gamma)}},$$
(B6)

where $T=gE/t_2,\,Y_1=g(t_1-\gamma)/t_2,\,Y_2=g(t_1+\gamma)/t_2.$ $\tau_1=a$ for $l\geq n,\,\tau_1=b$ for $l< n.\,\tau_2=a$ for $l>m,\,\tau_2=b$ for $l\leq m.$ For the zero modes E=0, we would have $x<-2|t_1|$, thus a and b are reduced to $-(t_1-\gamma)/t_2$ and $-(t_1+\gamma)/t_2$ for $-t_2+\gamma< t_1< t_2-\gamma,$ respectively. a and b are reduced to $-t_2/(t_1+\gamma)$ and $-t_2/(t_1-\gamma)$ for $t_1>t_2+\gamma$ or $t_1<-t_2-\gamma,$ respectively. Then Eq. (B5)and Eq. (B6) can be simplified as,

$$A_l/U_e = Y_3 \times \begin{cases} \left(-\frac{t_1 - \gamma}{t_2}\right)^{(l-m)}, & (l > m), \\ 0, & (l \le m), \end{cases}$$
 (B7)

$$B_l/U_e = Y_4 \times \begin{cases} \left(-\frac{t_1 + \gamma}{t_2}\right)^{(n-l)}, & (l < n), \\ 0, & (l \ge n), \end{cases}$$
(B8)

where $Y_3 = g/(t_1 - \gamma), Y_4 = g/(t_1 + \gamma)$.

Similarly, for the system with A - A coupling, Eq. (A6) yields

$$A_{k}/U_{e} = \frac{gE}{\sqrt{L}t_{2}} \left(e^{-ikn} + e^{-ikm}\right) f(k),$$

$$B_{k}/U_{e} = \frac{g\left(t_{1} - \gamma + t_{2}e^{ik}\right)}{\sqrt{L}t_{2}} \left(e^{-ikn} + e^{-ikm}\right) f(k).$$
(B9)

By the inverse Fourier transformation, we can obtain

$$A_l/U_e = \frac{1}{\sqrt{L}} \sum_k e^{ikl} A_k/U_e$$

$$= \frac{(-1)^{y+1}T}{\sqrt{x^2 - 4(t_1 + \gamma)(t_1 - \gamma)}} \left(\tau_1^{|l-n|} + \tau_3^{|l-m|}\right),$$

$$B_{l}/U_{e} = \frac{1}{\sqrt{L}} \sum_{k} e^{ikl} B_{k}/U_{e}$$

$$= \frac{(-1)^{y+1}}{\sqrt{x^{2} - 4(t_{1} + \gamma)(t_{1} - \gamma)}} \left\{ Y_{1} \left(\tau_{1}^{|l-n|} + \tau_{3}^{|l-m|} \right) + g \left(\tau_{1}^{|l-n+1|} + \tau_{3}^{|l-m+1|} \right) \right\},$$
(B11)

(B10)

where $\tau_3 = a$ for $l \geq m$, $\tau_3 = b$ for l < m. Then setting E=0, the Eq. (B10) and Eq. (B11) can be simplified as $A_l/U_e = 0$,

$$B_{l}/U_{e} = -Y_{4} \times \begin{cases} 0, & (l < n), \\ \left(\frac{-t_{2}}{t_{1}+\gamma}\right)^{l-n}, & (n \leq l < m), \\ \left(\frac{-t_{2}}{t_{1}+\gamma}\right)^{l-n} + \left(\frac{-t_{2}}{t_{1}+\gamma}\right)^{l-m}, & (m \leq l), \end{cases}$$
(B12)

for $t_1 > t_2 + \gamma$ or $t_1 < -t_2 - \gamma$, and

$$B_{l}/U_{e} = 0,$$

$$B_{l}/U_{e} = -Y_{4} \times \begin{cases} 0, & (l < n), \\ \left(\frac{-t_{2}}{t_{1} + \gamma}\right)^{l - n}, & (n \leq l < m), \\ \left(\frac{-t_{2}}{t_{1} + \gamma}\right)^{l - n} + \left(\frac{-t_{2}}{t_{1} + \gamma}\right)^{l - m}, & (m \leq l), \\ \left(\frac{-t_{2}}{t_{1} + \gamma}\right)^{l - n} + \left(\frac{-t_{2}}{t_{1} + \gamma}\right)^{l - m}, & (m \leq l), \\ (B12) & \text{for } -t_{2} + \gamma < t_{1} < t_{2} - \gamma. \end{cases}$$

- [1] E. Majorana. Sulla formazione dello ione molecolare dielio. Nuovo Cimento, 8, 22, (1931).
- [2] Herman Feshbach, Unified theory of nuclear reactions, Nuovo Cimento, Ann. Phys. (NY) 5, 357 (1958).
- [3] N. Hatano and D. R. Nelson, Localization Transitions in Non-Hermitian Quantum Mechanics, Phys. Rev. Lett. 77, 570
- [4] C. M. Bender and S. Boettcher, Real Spectra in Non-Hermitian Hamiltonians Having PT Symmetry, Phys. Rev. Lett. 80, 5243
- [5] M. V. Berry, Physics of non-Hermitian degeneracies, Czech. J. Phys. 54, 1039 (2004).
- N. Moiseyev, Non-Hermitian Quantum Mechanics, 1st ed. (Cambridge University Press, London, 2011).
- D. C. Brody, Biorthogonal quantum mechanics, J. Phys. A 47, 035305 (2013).
- [8] Midya Parto, Steffen Wittek, Hossein Hodaei, Gal Harari, Miguel A. Bandres, Jinhan Ren, Mikael C. Rechtsman, Edge-Mode Lasing in 1D Topological Active Arrays, Phys. Rev. Lett. 120, 113901 (2018).
- [9] S. Weimann, M. Kremer, Y. Plotnik, Y. Lumer, S. Nolte, K. G. Makris, M. Segev, M. C. Rechtsman, and A. Szameit, Topologically protected bound states in photonic parity-time-symmetric crystal, Nat. Mater. 16, 433 (2016).
- [10] M. A. Bandres, S. Wittek, G. Harari, M. Parto, J. Ren, M. Segev, D. N. Christodoulides, and M. Khajavikhan, Topological insulator laser: Experiments, Science 359, eaar4005 (2018).
- [11] S.-D. Liang, and G.-Y. Huang, Topological invariance and global Berry phase in non-Hermitian systems, Phys. Rev. A 87, 012118 (2013).
- [12] T. E. Lee, Anomalous edge state in a non-Hermitian lattice, Phys. Rev. Lett. 116, 133903 (2016).
- [13] D. Leykam, K. Y. Bliokh, C. Huang, Y. D. Chong, and F. Nori, Edge modes, degeneracies, and topological numbers in non-Hermitian systems, Phys. Rev. Lett. 118, 040401 (2017).
- [14] Z. Gong, Y. Ashida, K. Kawabata, K. Takasan, S. Higashikawa, and M. Ueda, Topological phases of non-Hermitian systems, Phys. Rev. X 8, 031079 (2018).
- [15] Tao Liu, Yu-Ran Zhang, Qing Ai, Zongping Gong, Kohei Kawabata, Masahito Ueda, and Franco Nori, Second-Order Topological Phases in Non-Hermitian Systems, Phys. Rev. Lett. **122**, 076801 (2019).
- [16] Chuanhao Yin, Hui Jiang, Linhu Li, Rong Lü, and Shu Chen, Geometrical meaning of winding number and its characterization of topological phases in one-dimensional chiral non-Hermitian systems, Phys, Rev A 97, 052115 (2018).
- [17] S. Lieu, Topological phases in the non-Hermitian Su-Schrieffer-Heeger model, Phys. Rev. B 97, 045106 (2018).
- [18] H. Shen, B. Zhen, and L. Fu, Topological band theory for non-

- Hermitian Hamiltonians, Phys. Rev. Lett. 120, 146402 (2018).
- Y. Xiong. Why does bulk boundary correspondence fail in some non-Hermitian topological models, J. Phys. Commun. 2, 035043 (2018).
- [20] Flore K. Kunst, Elisabet Edvardsson, Jan Carl Budich, and Emil J. Bergholtz, Biorthogonal Bulk-Boundary Correspondence in Non-Hermitian Systems, Phys. Rev. Lett. 121, 026808 (2018).
- Shunyu Yao, and Zhong Wang, Edge States and topological invariants of non-Hermitian systems, Phys. Rev. Lett. 121, 086803 (2018).
- Shunyu Yao, Fei Song, and Zhong Wang, Non-Hermitian Chern bands, Phys. Rev. Lett. 121, 136802 (2018).
- Fei Song, Shunyu Yao, and Zhong Wang, Non-Hermitian Skin Effect and Chiral Damping in Open Quantum Systems, Phys. Rev. Lett. 123, 170401 (2019).
- Fei Song, Shunyu Yao, and Zhong Wang, Non-Hermitian Topological Invariants in Real Space, Phys. Rev. Lett. 123, 246801 (2019).
- [25] Zhesen Yang, Kai Zhang, Chen Fang, and Jiangping Hu, Non-Hermitian Bulk-Boundary Correspondence and Auxiliary Generalized Brillouin Zone Theory, Phys. Rev. Lett. 125, 226402 (2020).
- [26] Kai Zhang, Zhesen Yang, and Chen Fang, Correspondence between Winding Numbers and Skin Modes in Non-Hermitian Systems, Phys. Rev. Lett. 125, 126402 (2020).
- [27] Yifei Yi, and Zhesen Yang, Non-Hermitian Skin Modes Induced by On-Site Dissipations and Chiral Tunneling Effect, Phys. Rev. Lett. 125, 186802 (2020).
- [28] Nobuyuki Okuma, Kohei Kawabata, Ken Shiozaki, and Masatoshi Sato, Topological Origin of Non-Hermitian Skin Effects, Phys. Rev. Lett. 124, 086801 (2020).
- [29] V. M. Martinez Alvarez, J. E. Barrios Vargas, and L. E. F. Foa Torres, Non-Hermitian robust edge states in one dimension: Anomalous localization and eigenspace condensation at exceptional points, Phys. Rev. B 97, 121401(R) (2018).
- [30] Ching Hua Lee, and Ronny Thomale, Anatomy of skin modes and topology in non-Hermitian systems, Phys. Rev. B 99, 201103(R) (2019).
- [31] Linhu Li, Ching Hua Lee, and Jiangbin Gong, Topological Switch for Non-Hermitian Skin Effect in Cold-Atom Systems with Loss, Phys. Rev. Lett. **124**, 250402 (2020).
- [32] Ching Hua Lee, Linhu Li, and Jiangbin Gong, Hybrid Higher-Order Skin-Topological Modes in Nonreciprocal Systems, Phys. Rev. Lett. 123, 016805 (2019).
- [33] Linhu Li, Ching Hua Lee, Sen Mu, and Jiangbin Gong, Critical non-Hermitian skin effect, , Nat. Commun. 11, 5491 (2020).
- Tobias Hofmann, Tobias Helbig, Frank Schindler, Nora Salgo, Marta Brzezińska, Martin Greiter, Tobias Kiessling, David Wolf, Achim Vollhardt, Anton Kabaši, Ching Hua Lee, Ante

- Bilušić, Ronny Thomale, and Titus Neupert, Reciprocal skin effect and its realization in a topolectrical circuit, Phys. Rev. Research **2**, 023265 (2020).
- [35] Lei Xiao, Tianshu Deng, Kunkun Wang, Gaoyan Zhu, Zhong Wang, Wei Yi, and Peng Xue, Non-Hermitian bulk-boundary correspondence in quantum dynamics, Nat. Phys. 16, 761-766 (2020).
- [36] T. Helbig, T. Hofmann, S. Imhof, M. Abdelghany, T. Kiessling, L. W. Molenkamp, C. H. Lee, A. Szameit, M. Greiter and R. Thomale, Generalized bulk-boundary correspondence in non-Hermitian topolectrical circuits, Nat. Phys. 16, 747-750 (2020).
- [37] Martin Brandenbourger, Xander Locsin, Edan Lerner, and Corentin Coulais, Non-reciprocal robotic metamaterials, Nat. Commun. 10, 4608 (2019).
- [38] Linhu Li, Ching Hua Lee, and Jiangbin Gong, Impurity induced scale-free localization, Commun. Phys. 4, 42 (2021).
- [39] Kazuki Yokomizo, and Shuichi Murakami, Scaling rule for the critical non-Hermitian skin effect, Phys. Rev. B 104, 165117 (2021).
- [40] Cui-Xian Guo, Chun-Hui Liu, Xiao-Ming Zhao, Yanxia Liu, and Shu Chen, Exact Solution of Non-Hermitian Systems with Generalized Boundary Conditions: Size-Dependent Boundary Effect and Fragility of the Skin Effect, Phys. Rev. Lett. 127, 116801 (2021).
- [41] Yanxia Liu and Shu Chen, Diagnosis of bulk phase diagram of nonreciprocal topological lattices by impurity modes, Phys. Rev. B 102, 075404 (2020).
- [42] Federico Roccati, Non-Hermitian skin effect as an impurity problem, Phys. Rev. A 104, 022215 (2021).
- [43] J. Lu, W.-Y. Shan, H.-Z. Lu, and S.-Q. Shen, Non-magnetic impurities and in-gap bound states in topological insulators, New J. Phys. 13, 103016 (2011).

- [44] R.-J. Slager, L. Rademaker, J. Zaanen, and L. Balents, Impurity-bound states and Green's function zeros as local signatures of topology, Phys. Rev. B 92, 085126 (2015).
- [45] B. Kannan, M. J. Ruckriegel, D. L. Campbell, A. F. Kockum, J. Braumüller, D. K. Kim, M. Kjaergaard, P. Krantz, A. Melville, B. M. Niedzielski, A. Vepsäläinen, R. Winik, J. L. Yoder, F. Nori, T. P. Orlando, S. Gustavsson, and W. D. Oliver, Waveguide quantum electrodynamics with superconducting artificial giant atoms, Nature (London) 583, 775 (2020).
- [46] R. Manenti, A. F. Kockum, A. Patterson, T. Behrle, J. Rahamim, G. Tancredi, F. Nori, and P. J. Leek, Circuit quantum acoustodynamics with surface acoustic waves, Nat. Commun. 8, 975 (2017).
- [47] L. R. Sletten, B. A. Moores, J. J. Viennot, and K. W. Lehnert, Resolving Phonon Fock States in a Multimode Cavity with a Double-Slit Qubit, Phys. Rev. X 9, 021056 (2019).
- [48] Xin Wang, Tao Liu, Anton Frisk Kockum, Hong-Rong Li, and Franco Nori, Tunable Chiral Bound States with Giant Atoms, Phys. Rev. Lett. 126, 043602 (2021).
- [49] Weijun Cheng, Zhihai Wang, and Yu-xi Liu, Boundary effect and dressed states of a giant atom in a topological waveguide, arXiv: 2103.04542.
- [50] G. Andersson, M. K. Ekström, and P. Delsing, Electromagnetically Induced Acoustic Transparency with a Superconducting Circuit, Phys. Rev. Lett. 124, 240402 (2020).
- [51] G. Dee and J. S. Langer, Propagating Pattern Selection, Phys. Rev. Lett. 50, 383 (1983).
- [52] S. Longhi, Convective and absolute PT -symmetry breaking in tight-binding lattices, Phys. Rev. A 88, 052102 (2013).
- [53] S. Longhi, Probing non-Hermitian skin effect and non-Bloch phase transition, Phys. Rev. Research 1, 023013 (2019).